Hindawi Publishing Corporation
International Journal of Photoenergy
Volume 2014, Article ID 176835, 8 pages
http://dx.doi.org/10.1155/2014/176835

Research Article

Microwave Synthesis of Zinc Oxide/Reduced Graphene Oxide Hybrid for Adsorption-Photocatalysis Application

Fatin Saiha Omar,[1] Huang Nay Ming,[1] Syed Muhamad Hafiz,[1] and Lim Hong Ngee[2,3]

[1] *Department of Physics, Low Dimensional Materials Research Centre, Faculty of Science, University of Malaya, 50603 Kuala Lumpur, Malaysia*
[2] *Department of Chemistry, Faculty of Science, Universiti Putra Malaysia (UPM), 43400 Serdang, Selangor, Malaysia*
[3] *Functional Device Laboratory, Institute of Advanced Technology, Universiti Putra Malaysia (UPM), 43400 Serdang, Selangor, Malaysia*

Correspondence should be addressed to Huang Nay Ming; huangnayming@gmail.com
and Lim Hong Ngee; janet_limhn@yahoo.com

Received 4 November 2013; Accepted 9 December 2013; Published 2 January 2014

Academic Editor: Lizhi Zhang

Copyright © 2014 Fatin Saiha Omar et al. This is an open access article distributed under the Creative Commons Attribution License, which permits unrestricted use, distribution, and reproduction in any medium, provided the original work is properly cited.

This work reports on synthesis of zinc oxide/reduced graphene oxide (ZnO/rGO) nanocomposites in the presence of diethylenetriamine (DETA) via a facile microwave method. The X-ray diffraction (XRD) patterns of the nanocomposites correspond to the ZnO hexagonal phase wurtzite structure. The high-resolution transmission electron microscopy (HRTEM) images revealed that the ZnO nanorods, with an average length : diameter ratio of 10, were successfully deposited on the rGO sheets. Under the irradiation of sunlight, the nanocomposites showed enhanced adsorption-photocatalysis by more than twofold and photocurrent response by sixfold compared to the ZnO. The excellent photoactivity performance of the nanocomposites is contributed by smaller ZnO nanorod and the presence of rGO that acts as a photosensitizer by transferring electrons to the conduction band of ZnO within the nanocomposite during sunlight illumination.

1. Introduction

Direct discharge of pigments and dyes by textile industries into waters endangers the aquatic lives. The colours block the sunlight from passing through the water, causing disturbance to the natural growth cycles of the living organisms in the waters. The heavy metals and organic and inorganic complexes used in the making of pigments and dyes are highly toxic and will accumulate in the fat deposits of large fishes which will be consumed by organisms in the higher order on land. Conventional biological treatments are only effective to adsorb the dye, causing secondary pollution [1, 2].

Photocatalysis is a method used to eliminate organic compounds in wastewater by mineralizing them into the simplest compounds like water and carbon monoxide. Semiconductor photocatalysts have been studied extensively because of favorable combination of electronic structure, light absorption properties, and charge transport characteristics. ZnO has been known as a suitable alternative to TiO_2 because of its strong oxidizing power, nontoxicity, and being relatively inexpensive. Its wide band gap (3.37 eV) and higher electron mobility hamper its use as a photocatalyst [3–6].

In an effort to improve the photocatalytic efficiency of ZnO, it has been doped, loaded, and combined with metals, nonmetals, and semiconductors [7–10]. Recently, researchers are astounded with graphene because of its unique electronic properties and large theoretical specific surface area. These properties make graphene a good candidate for combination with the ZnO because graphene's pristine mechanical performance stabilizes catalysis and offers a two-dimensional plane to deposit catalyst [11]. Transport through delocalized conjugated π structures allows charge carriers in graphene to achieve high mobility and relatively slow charge recombination. Attempts to fabricate ZnO/rGO composite have been reported to obtain superior properties [12–15]. In photocatalysis, ZnO can act as a photocatalyst while graphene

acts as an electron-acceptor/transport material to facilitate the migration of photogenerated electrons and hinder the electron-hole recombination [16, 17]. Besides that, it has also been known to be an excellent adsorber for organic compounds [18].

In this work, a microwave approach was used to synthesize ZnO/rGO. Microwave radiation provides a fast and uniform heating rate that can cause rapid particles nucleation and growth which can reduce the reaction time, and therefore it can save a large amount of energy [19]. Diethylenetriamine (DETA) plays a role as a stabilizer by controlling the final morphology of the samples [20]. The defects in graphene oxide act as heterogeneous active sites for the nucleation and growth of ZnO particles [21]. The adsorption and photodegradation of methylene blue (MB) and photocurrent of the ZnO/rGO nanocomposites were investigated. Photocurrent is evidence to demonstrate the behavior of charge carriers within the samples under irradiation which can be correlated with the photocatalytic activity [22].

2. Experimental

2.1. Materials. Graphite flakes were purchased from Ashbury Inc. Zinc acetate dehydrate ($Zn(CH_3COO)_2{\cdot}2H_2O$) was purchased from Bendosen. Diethylenetriamine ($HN(CH_2CH_2NH_2)_2$) was purchased from Merck. Sodium hydroxide (NaOH), potassium permanganate ($KMnO_4$), sulfuric acid (H_2SO_4), and acid hydrochloric (HCl) were purchased from R&M Marketing. Hydrogen peroxide (H_2O_2) and methylene blue were purchased from Systerm. Distilled water was used throughout the sample preparation.

2.2. Methods

2.2.1. Synthesis of ZnO/rGO Photocatalyst. Graphite powder was used as the starting reagent to synthesize GO using a simplified Hummer's method. 20 μL of DETA was dropped into 4.6 mM ($Zn(CH_3COO)_2{\cdot}2H_2O$) solution and then was stirred for 30 min. Certain amount of 14 mg/mL GO gel was sonicated in distilled water to produce uniform dispersion. Under stirring, the zinc solution was added dropwise into GO solution at a rate of a drop per 5 sec followed by 0.09 M NaOH until reaching pH value of 12 and stirred for 13 h. The mixture was then placed in a microwave and treated for 30 min. After letting it cool at room temperature, the precipitates were washed three times with distilled water and finally dried in oven at 60°C for 24 h. Three kinds of composite obtained with different GO loadings, 0.2, 0.7, and 1.5 wt% GO gel, were named as ZG3, ZG2, and ZG1, respectively. ZnO was synthesized using the similar procedure. For comparison purpose, composite without DETA was also prepared using the similar procedure and named as ZG.

2.3. Characterizations. The structure and morphology of the samples were characterized by X-ray diffractometry (XRD) Philips D5000 using CuKα radiation (λ = 1.4506 Å), field emission scanning electron microscope (FESEM) JSM-7600F, and high-resolution transmission electron microscope (HRTEM) JEM-2100F. Ultraviolet-visible absorption spectra were recorded using UV-vis spectroscopy Thermo scientific Evolution 300. Raman spectra were recorded using a Renishaw inVia Raman microscope system.

2.4. Photocatalytic Experiments. The photocatalytic properties of the samples were evaluated by photodegradation of MB solution under natural sunlight. In every experiment, 5 mg of photocatalyst was exposed to natural sunlight under magnetic stirring in 10 mL of 5 ppm MB. Prior to irradiation, the suspensions were stirred in the dark overnight to achieve a saturated adsorption between the photocatalysts and MB molecules. The loaded samples were used repeatedly, and each cycle lasted for 2 h. Before the next cycle, the remaining solution was replaced with fresh MB solution. Tow mL solution was withdrawn every 20 min, and the concentration of MB solution was measured within 450 nm to 750 nm using a UV-Vis spectrometer. The change of relative absorbance was used to record the change of concentration of MB solution, that was *Ct/Co* (*Ct* referred to the concentration of MB solution at time *t* and *Co* referred to the concentration of MB solution at initial time). All experiments were repeated six times.

2.5. Photocurrent Preparation. To investigate the transition of photogenerated electrons before and after the rGO loading, ZnO and ZnO/rGO electrodes were prepared as follows: 0.5 mg of the as-prepared photocatalyst was mixed in distilled water to produce slurry form, which was then smeared onto a 1 cm × 1 cm indium-tin oxide (ITO) glass using doctor blade's method. The coated ITO glass was dried in the oven at 60°C for 24 h. All investigated electrodes were of similar mass and exposed area.

The photocurrents were carried out using a VersaSTAT 3 potentiostat (Ametek Princeton Applied Research, Oak Ridge, TN). A solar light simulator Oriel Instrument was used to simulate sunlight under one sun AM 1.5 G with the measured light irradiance of 100 mW cm^{-2} provided by a 150 W xenon light source. A conventional three-electrode cell with working electrode (as-prepared photocatalyst), a platinum wire as counter electrode, an Ag/AgCl (in 3 M KCl) as reference electrode, and 1 M KCl as electrolyte was used. The photoresponse of the photocatalysts as light on and off were measured at 0.5 V.

3. Results and Discussion

Figure 1 shows the XRD patterns of ZnO, ZG1, ZG2, ZG3, rGO, and GO. All the diffraction peaks of ZnO are consistent with the hexagonal phase wurtzite structure (JCPDS number 80-0074). The peak (002) of GO at 11.1° is ascribed to the introduction of oxygenated functional groups attached on both sides and edges of carbon sheets [23]. Meanwhile, the diffraction peaks of the nanocomposites are similar to those of ZnO. The disappearance of the GO peak suggests the complete exfoliation of GO due to the insertion of ZnO particles [24]. No diffraction peak of rGO can be observed in the nanocomposites, which might be due to the low amount

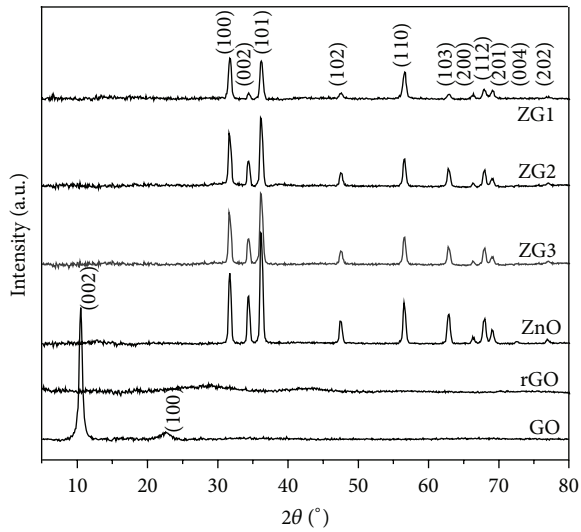

Figure 1: XRD patterns of GO, rGO, ZnO, ZG1, ZG2, and ZG3.

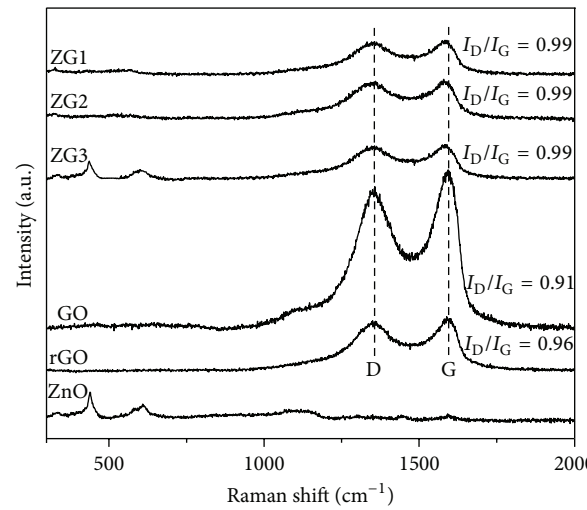

Figure 3: Raman spectra of GO, rGO, ZnO, ZG1, ZG2, and ZG3.

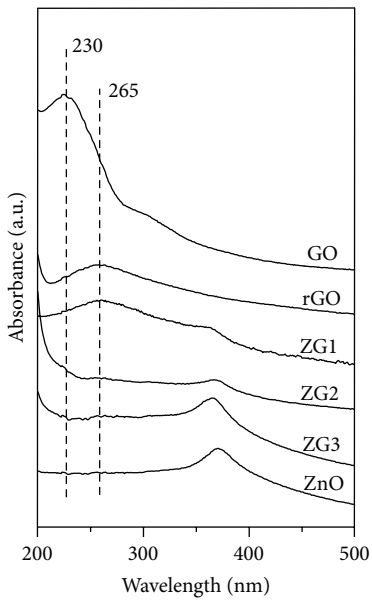

Figure 2: UV-Vis spectra of GO, rGO, ZnO, ZG1, ZG2, and ZG3.

and the extensive exfoliation of rGO. The reduction of GO is confirmed by the appearance of small bumps at 29° and 44°, indicating the removal of a large number of oxygen-containing groups and the formation of much more disordered graphene sheets [25]. No other peak of impurity is detected.

Figure 2 shows the UV-Vis absorption spectra of ZnO, ZG1, ZG2, ZG3, rGO, and GO. The spectra of GO exhibit a maximum absorption peak at 230 nm, corresponding to the $\pi \rightarrow \pi$ transition of the aromatic C–C bonds [26]. After the reduction of the GO, the absorption peak had red-shifted to 265 nm, indicating restoration of π conjugation within the rGO sheets [27]. The ZnO shows an absorption peak at 360 nm which can also be observed in the nanocomposites which suggests the presence of ZnO nanostructures [28]. Besides, the red shift of the ZnO absorption edge in the nanocomposites is ascribed to the chemical interaction between ZnO and rGO [29]. Comparing ZG1, ZG2, and ZG3, the relative intensity of the carbon peak (~265 nm) increases with rGO loading in the nanocomposites.

The presence of both carbon and ZnO can be confirmed from the Raman spectra. In Figure 3, the spectrum for ZnO displays a peak at 330 cm^{-1} which is assigned to the second-order Raman spectrum arising from zone-boundary phonons of hexagonal ZnO. The intense peak at 440 cm^{-1} corresponds to $E2$ (HI) mode, which is the characteristic peak of the hexagonal wurtzite phase ZnO. The peak at 582 cm^{-1} is assigned to $E1$ (LO) mode, attributed to oxygen deficiency defects in ZnO [30]. The peak at 1130 cm^{-1} is due to the multiple-phonon scattering processes [31]. The intensity of these peaks is reduced in composites as compared to that in ZnO due to the interaction between ZnO and rGO.

The similar G and D band (where G peak refers to the presence of sp^2 carbon-type structure and D peak refers to the presence of disorder in the graphene structure [32]) for rGO and nanocomposites suggests that the structure of rGO is maintained in the composites. The D/G intensity value of the nanocomposites (0.99) increased compared with that of the GO (0.91) and rGO (0.96). The nanocomposite exhibits the highest D/G value due to the increasing disorder of sp^2 contributed by the presence of ZnO in the composites [33, 34]. Compared with rGO, the D band was blue-shifted by 4 cm^{-1} while the G band was blue-shifted by 10 cm^{-1} in nanocomposites. These shifts are attributed to the chemical interaction between ZnO and rGO [35].

Figure 4(a) compares the C1s peak of GO and ZG1 nanocomposite. Both peaks can be deconvoluted into four Gaussian peaks, namely, sp^2 carbon (C–C, 284.5 eV), C–O (286 eV), C=O (287.4 eV), and O–C=O (288.8 eV). The peak intensity of the oxygen-bonded carbon reduced in the composite, indicating the reduction of GO after the microwave

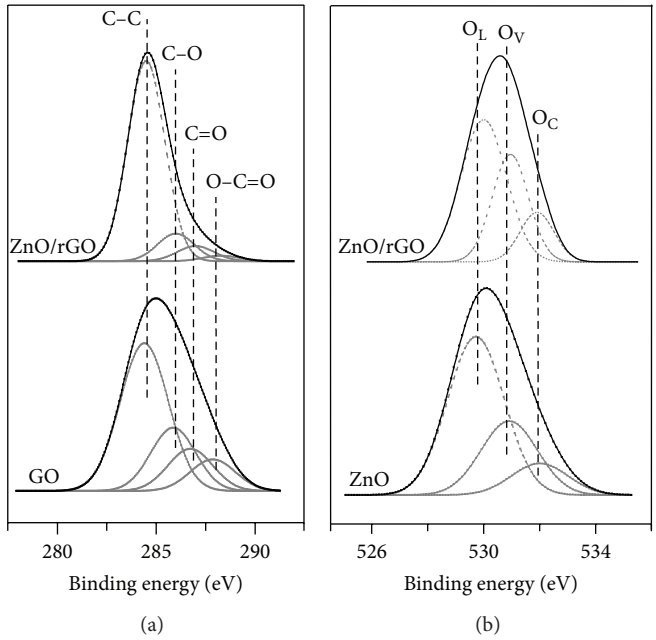

Figure 4: XPS spectra of (a) C1s of GO and ZG1 and (b) O1s of ZnO and ZG1.

treatment [36]. Figure 4(b) shows the O1s peak of ZnO and nanocomposite. The XPS pattern of ZnO can be deconvoluted into three Gaussian peaks, O_L (oxygen lattice, 529.8 eV), O_V (oxygen vacancy, 531 eV), and O_C (chemisorbed oxygen species, 532.1 eV). The first two peaks are attributed to O^{2-} ion in the Zn–O bonds and oxygen deficient defects, respectively. The last peak is assigned to the presence of loosely bound oxygen such as adsorbed O_2 and H_2O on the ZnO surface. The O1s peaks of the nanocomposite have slightly higher binding energies than ZnO, with the deconvoluted peaks positioned at 530, 531.2, and 532.3 eV. Notice that the nanocomposite shows higher intensity on the second peak compared to ZnO, indicating an increased density of oxygen vacancy on the ZnO surface. Oxygen vacancy could act as an electron trap that could hinder the electron-hole recombination and in turn could help in effective photocatalytic degradation [37].

As shown in Figure 5, individual ZnO and ZnO in the nanocomposites are rod-like with an average diameter and length of 100 nm and 1 μm, respectively. The nanocomposite in the absence of DETA (Figure 5(c)) shows that the size of the ZnO nanorod is bigger compared to the nanocomposite with DETA (Figure 5(b)). This is due to the interaction between Zn^{2+} with DETA that formed Zn-DETA complex. The Zn-DETA complex hindered the fast reaction of Zn^{2+} with OH^-, forming ZnO nanorods with smaller diameter [38].

Figure 6 revealed that, for ZnO, the nanorods apparently originate from a centre, forming flower-like morphologies. Meanwhile, the ZnO rods are distributed on the surface of rGO for all the nanocomposites, confirming the interaction between ZnO and rGO. The average diameter of the ZnO nanorods in the nanocomposite is slightly decreased with increasing rGO content due to the higher number of reaction sites provided by the GO that inhibited the agglomeration of ZnO particles [39]. The smaller size of the ZnO in the nanocomposites provides larger effective surface area in the enhancement of photocatalytic activity [40]. The crystal lattice fringes (Figure 6(e)) with a d-spacing of 0.26 nm can be assigned to the (002) plane of hexagonal ZnO [41].

4. Photocatalysis

Adsorption of the dye is an important parameter in determining the photodegradation rate. To distinguish the functions of the adsorption of rGO and photocatalysis of ZnO, the suspension was stirred overnight in the dark to reach the saturated adsorption of MB before illumination.

Based on Figure 7(a), the ZnO shows 3% of MB adsorption. When rGO is introduced to ZnO, the adsorption rate increased to 45.7%, 64.9%, and 82.3% for ZG3, ZG2, and ZG1, respectively. The enhancement of MB absorption increased with increasing proportion of rGO in the nanocomposites which is attributed to the π-π stacking interactions between MB and rGO [42]. In Figure 7(b), the degradation rates for blank (without photocatalyst) ZG, ZnO, ZG3, ZG2, and ZG1 are 12%, 25%, 39.4%, 63.5%, 75.4%, and 94.8%, respectively. The observed enhanced photocatalytic activity by the nanocomposites is largely attributed to the smaller diameter of the ZnO nanorod providing larger effective surface area that improves the absorbance of MB and the presence of rGO that acts as a photosensitizer. rGO is photoexcited by sunlight and transfers electrons to the CB of ZnO, raising the concentration of electrons leading to dye degradation [43].

The stability of photocatalyst during photocatalysis is a crucial factor for practical application. The reusability of ZG1 in photodegradation of MB is tested by repeating the photocatalytic experiment for six cycles after the completion of the photocatalytic experiment shown in Figure 7. In Figure 8(a), MB solution was almost completely adsorbed

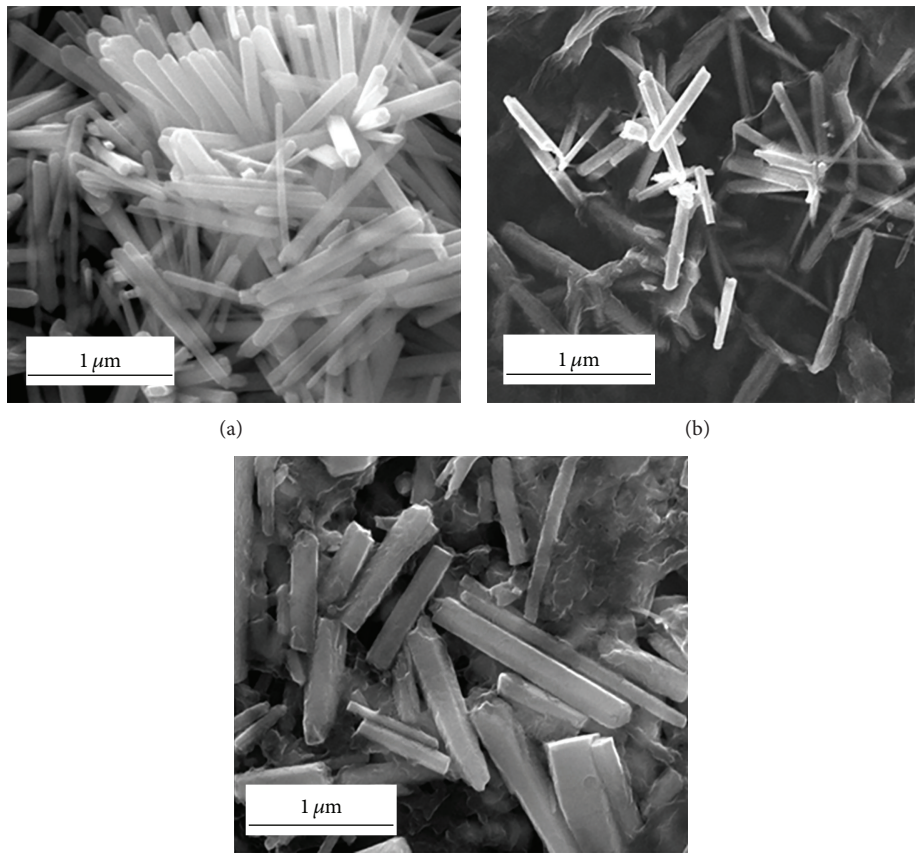

(a) (b)

(c)

Figure 5: FESEM images of (a) ZnO, (b) ZG1, and (c) ZG.

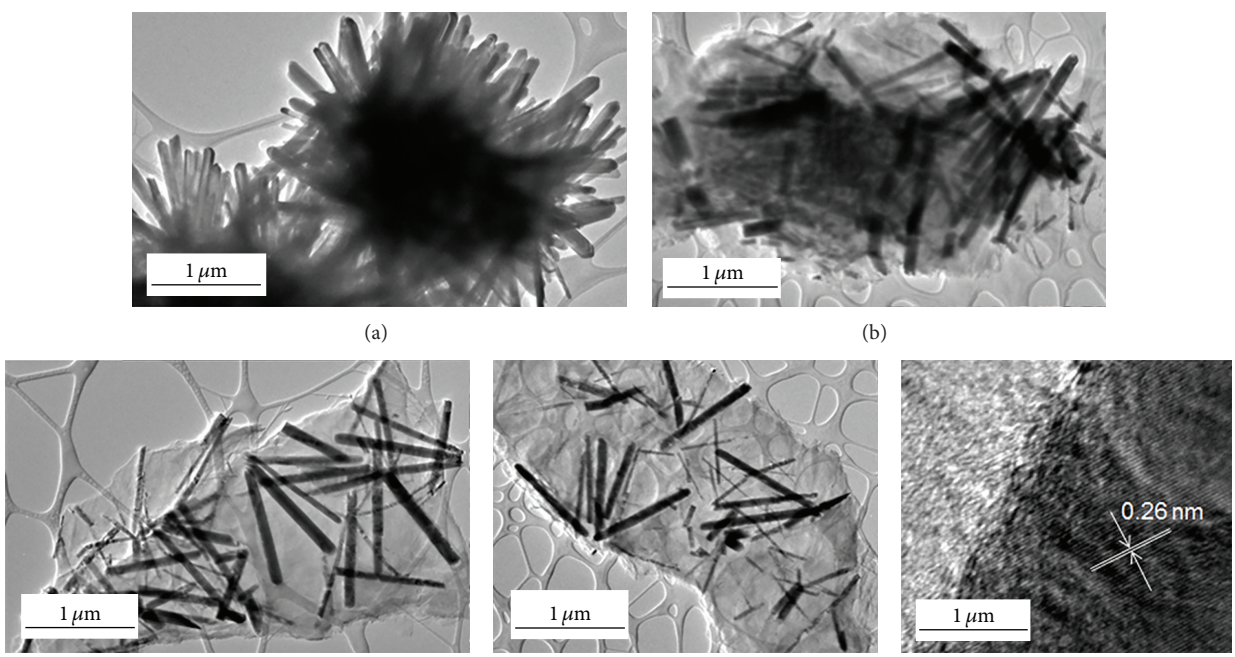

(a) (b)

(c) (d) (e)

Figure 6: HRTEM images of (a) ZnO, (b) ZG3, (c) ZG2, (d) ZG1, and (e) ZG1 at a higher magnification.

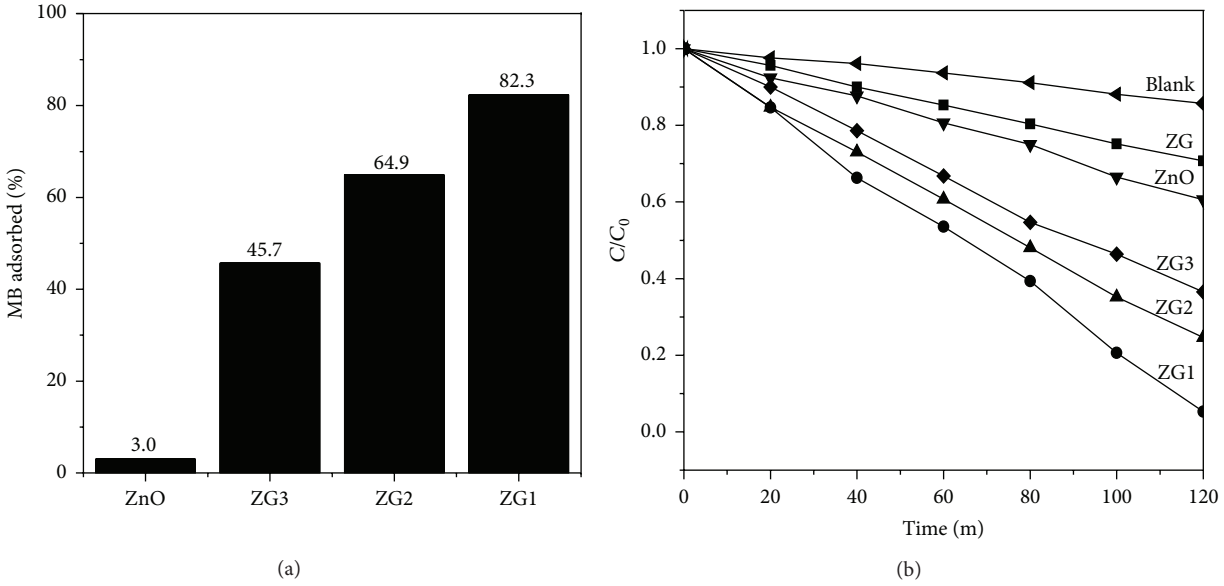

Figure 7: (a) Adsorption performance of ZnO, ZG1, ZG2, and ZG3 in the dark. (b) Photodegradation performance of blank (without photocatalyst) ZnO, ZG, ZG1, ZG2, and ZG3 under the sunlight.

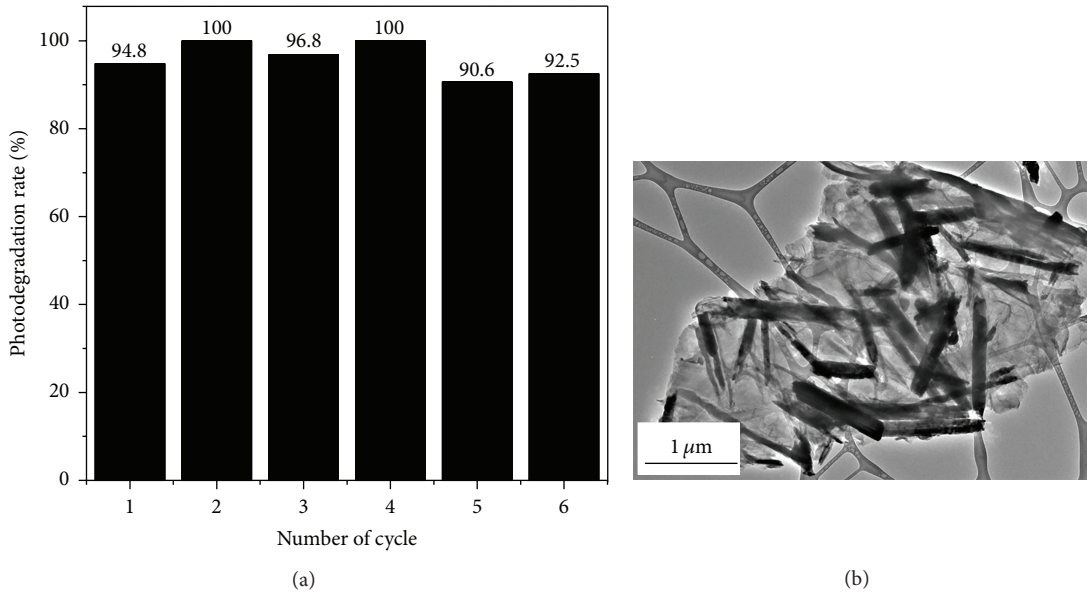

Figure 8: (a) Cycling runs in the photodegradation of MB by ZG1 under the sunlight. (b) HRTEM image of ZG1 for cycles.

and degraded by ZG1 for each cycle. ZG1 does not exhibit any changes in morphology even after the sixth cycle, revealing that it is photostable (Figure 8(b)).

4.1. Photocurrent. All the nanocomposites exhibit much higher photocurrent intensity than ZnO, where the photocurrent of ZG1 is about eight times higher than that of ZnO (Figure 9). The photocurrents are 6.0 μA cm^{-2}, 7.5 μA cm^{-2}, 11.0 μA cm^{-2}, 17.5 μA cm^{-2}, and 24.7 μA cm^{-2} for ZnO, ZG, ZG3, ZG2, and ZG1, respectively. The generated photocurrent increased with the increase of the concentration of rGO, attributed to the extra electrons injection from the excited rGO within the nanocomposites under illumination [44]. These results are in agreement with the photocatalysis results (Figure 7(b)), where the rGO is photoexcited by sunlight, increasing the amount of electrons in the nanocomposite. This also shows that the nanocomposite could be applied as photoelectrochemical material for light-induced hydrogen evolution as photoinduced electrons and holes can participate in a redox reaction.

5. Conclusions

ZnO/rGO nanocomposites were successfully synthesized via a facile microwave method in the presence of DETA. The stability of coordination structure between Zn^{2+} and DETA

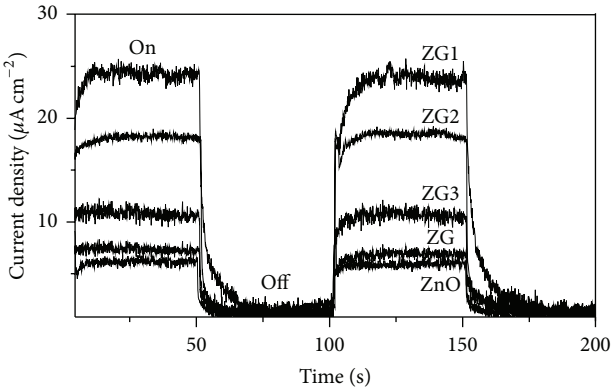

FIGURE 9: Photocurrent of ZnO, ZG, ZG1, ZG2, and ZG3 under solar light irradiation. ([KCl] = 1 M).

plays an important role for the final morphology of the ZnO and ZnO/rGO nanocomposites. The adsorption and photocatalytic activities of the nanocomposites are dependent on the proportion of rGO loading in the samples. The nanocomposites outperformed ZnO due to synergistic effects of smaller ZnO nanorod and the presence of rGO that acts as a photosensitizer during sunlight illumination. It is also evident that the nanocomposite is stable as it displays consistent recycling for up to six runs. The nanocomposites show significantly higher photocurrent response than ZnO, which is in agreement with the photocatalysis result, which manifest the possibility of using the nanocomposite for real application in wastewater treatment.

Conflict of Interests

The authors declare that there is no conflict of interests regarding the publication of this paper.

Acknowledgments

This work was supported by the High Impact Research Grant under the Ministry of Higher Education of Malaysia (UM.C/625/1/HIR/MOHE/05), L'Oréal Malaysia "For Women in Science Fellowships" 2011 (6375900-10501), and Postgraduate Research Fund (PG107-2012B).

References

[1] A. K. Asiagwu, "Sorption model for the removal of m-anisidine dye from aqueous solution using beaker's yeast (*Saccharomuces cerevisiae*)," *International Journal of Research and Reviews in Applied Sciences*, vol. 13, pp. 617–625, 2012.

[2] E. S. Beach, R. T. Malecky, R. R. Gil, C. P. Horwitz, and T. J. Collins, "Fe-TAML/hydrogen peroxide degradation of concentrated solutions of the commercial azo dye tartrazine," *Catalysis Science and Technology*, vol. 1, no. 3, pp. 437–443, 2011.

[3] A. K. Singh, S. S. Multani, and S. B. Patil, "ZnO nanorods and nanopolypods synthesized using microwave assisted wet chemical and thermal evaporation method," *Indian Journal of Pure and Applied Physics*, vol. 49, no. 4, pp. 270–276, 2011.

[4] M. Gusatti, J. D. A. do Rosário, C. E. M. de Campos et al., "Production and characterization of ZnO nanocrystals obtained by solochemical processing at different temperatures," *Journal of Nanoscience and Nanotechnology*, vol. 10, no. 7, pp. 4348–4351, 2010.

[5] S. Xu and Z. L. Wang, "One-dimensional ZnO nanostructures: solution growth and functional properties," *Nano Research*, vol. 4, no. 11, pp. 1013–1098, 2011.

[6] Y. Yang, L. Ren, C. Zhang, S. Huang, and T. Liu, "Facile fabrication of functionalized graphene sheets (FGS)/ZnO nanocomposites with photocatalytic property," *ACS Applied Materials and Interfaces*, vol. 3, no. 7, pp. 2779–2785, 2011.

[7] N. P. Mohabansi, V. B. Patil, and N. Yenkie, "A comparative study on photo degradation of methylene blue dye effluent by advanced oxidation process by using TiO_2/ZnO photo catalyst," *Rasayan Journal of Chemistry*, vol. 4, no. 4, pp. 814–819, 2011.

[8] J. B. Zhong, J. Z. Li, X. Y. He et al., "Improved photocatalytic performance of Pd-doped ZnO," *Current Applied Physics*, vol. 12, no. 3, pp. 998–1001, 2012.

[9] M.-K. Lee and H.-F. Tu, "Au-ZnO and Pt-ZnO films prepared by electrodeposition as photocatalysts," *Journal of the Electrochemical Society*, vol. 155, no. 12, pp. D758–D762, 2008.

[10] J. V. Foreman, J. Li, H. Peng, S. Choi, H. O. Everitt, and J. Liu, "Time-resolved investigation of bright visible wavelength luminescence from sulfur-doped ZnO nanowires and micropowders," *Nano Letters*, vol. 6, no. 6, pp. 1126–1130, 2006.

[11] X. Zhou, T. Shi, and H. Zhou, "Hydrothermal preparation of ZnO-reduced graphene oxide hybrid with high performance in photocatalytic degradation," *Applied Surface Science*, vol. 258, no. 17, pp. 6204–6211, 2012.

[12] A. R. Marlinda, N. M. Huang, M. R. Muhamad et al., "Highly efficient preparation of ZnO nanorods decorated reduced graphene oxide nanocomposites," *Materials Letters*, vol. 80, pp. 9–12, 2012.

[13] W. Zou, J. Zhu, Y. Sun, and X. Wang, "Depositing ZnO nanoparticles onto graphene in a polyol system," *Materials Chemistry and Physics*, vol. 125, no. 3, pp. 617–620, 2011.

[14] W.-T. Song, J. Xie, S.-Y. Liu et al., "Graphene decorated with ZnO nanocrystals with improved electrochemical properties prepared by a facile in situ hydrothermal route," *International Journal of Electrochemical Science*, vol. 7, no. 3, pp. 2164–2174, 2012.

[15] W. Zou, J. Zhu, and X. Wang, "Preparation and characterization of graphene oxide-ZnO nanocomposites," *Materials Science Forum*, vol. 688, pp. 228–232, 2011.

[16] T. Lv, L. Pan, X. Liu et al., "One-step synthesis of CdS-TiO_2-chemically reduced graphene oxide composites via microwave-assisted reaction for visible-light photocatalytic degradation of methyl orange," *Catalysis Science and Technology*, vol. 2, no. 4, pp. 754–758, 2012.

[17] P. D. Tran, S. K. Batabyal, S. S. Pramana, J. Barber, L. H. Wong, and S. C. J. Loo, "A cuprous oxide-reduced graphene oxide (Cu_2O-rGO) composite photocatalyst for hydrogen generation: employing rGO as an electron acceptor to enhance the photocatalytic activity and stability of Cu_2O," *Nanoscale*, vol. 4, pp. 3875–3878, 2012.

[18] X. Dou, "Is graphene brand new in carbon-based semiconductor photocatalysts for organic pollutants degradation?" *Journal of Thermodynamics and Catalysis*, vol. 3, pp. 1–2, 2013.

[19] Y. Zheng, K. Lv, Z. Wang, K. Deng, and M. Li, "Microwave-assisted rapid synthesis of anatase TiO_2 nanocrystals with

exposed 001 facets," *Journal of Molecular Catalysis A*, vol. 356, pp. 137–143, 2012.

[20] W.-T. Yao, S.-H. Yu, S.-J. Liu, J.-P. Chen, X.-M. Liu, and F.-Q. Li, "Architectural control syntheses of CdS and CdSe nanoflowers, branched nanowires, and nanotrees via a solvothermal approach in a mixed solution and their photocatalytic property," *Journal of Physical Chemistry B*, vol. 110, no. 24, pp. 11704–11710, 2006.

[21] X. Xu, Y. Zhou, T. Yuan, and Y. Li, "Methanol electrocatalytic oxidation on Pt nanoparticles on nitrogen doped graphene prepared by the hydrothermal reaction of graphene oxide with urea," *Electrochimica Acta*, vol. 112, pp. 587–595, 2013.

[22] Y. Liu, C. Xie, J. Li, T. Zou, and D. Zeng, "New insights into the relationship between photocatalytic activity and photocurrent of TiO_2/WO_3 nanocomposite," *Applied Catalysis A*, vol. 433-434, pp. 81–87, 2012.

[23] Y. Li, W. Gao, L. Ci, C. Wang, and P. M. Ajayan, "Catalytic performance of Pt nanoparticles on reduced graphene oxide for methanol electro-oxidation," *Carbon*, vol. 48, no. 4, pp. 1124–1130, 2010.

[24] S. V. Kumar, N. M. Huang, N. Yusoff, and H. N. Lim, "High performance magnetically separable graphene/zinc oxide nanocomposite," *Materials Letters*, vol. 93, pp. 411–414, 2013.

[25] G. Singh, A. Choudhary, D. Haranath et al., "ZnO decorated luminescent graphene as a potential gas sensor at room temperature," *Carbon*, vol. 50, no. 2, pp. 385–394, 2012.

[26] Y. K. Kim and D. H. Min, "Simultaneous reduction and functionalization of graphene oxide by polyallylamine for nanocomposite formation," *Carbon Letters*, vol. 13, pp. 29–33, 2012.

[27] J. Yang and S. Gunasekaran, "Electrochemically reduced graphene oxide sheets as high performance supercapacitors," *Carbon*, vol. 51, pp. 36–44, 2013.

[28] Y. Yang and T. Liu, "Fabrication and characterization of graphene oxide/zinc oxide nanorods hybrid," *Applied Surface Science*, vol. 257, no. 21, pp. 8950–8954, 2011.

[29] X. Liu, L. Pan, Q. Zhao et al., "UV-assisted photocatalytic synthesis of ZnO-reduced graphene oxide composites with enhanced photocatalytic activity in reduction of Cr(VI)," *Chemical Engineering Journal*, vol. 183, pp. 238–243, 2012.

[30] J. Y. Li and H. Li, "Physical and electrical performance of vapor-solid grown ZnO straight nanowires," *Nanoscale Research Letters*, vol. 4, no. 2, pp. 165–168, 2009.

[31] X.-Y. Ye, Y.-M. Zhou, Y.-Q. Sun, J. Chen, and Z.-Q. Wang, "Preparation and characterization of Ag/ZnO composites via a simple hydrothermal route," *Journal of Nanoparticle Research*, vol. 11, no. 5, pp. 1159–1166, 2009.

[32] A. C. Ferrari, "Raman spectroscopy of graphene and graphite: disorder, electron-phonon coupling, doping and nonadiabatic effects," *Solid State Communications*, vol. 143, no. 1-2, pp. 47–57, 2007.

[33] S. Stankovich, D. A. Dikin, R. D. Piner et al., "Synthesis of graphene-based nanosheets via chemical reduction of exfoliated graphite oxide," *Carbon*, vol. 45, no. 7, pp. 1558–1565, 2007.

[34] J. Yang, X. Zhao, X. Shan et al., "Blue-shift of UV emission in ZnO/graphene composites," *Journal of Alloys and Compounds*, vol. 556, pp. 1–5, 2013.

[35] T. Xu, L. Zhang, H. Cheng, and Y. Zhu, "Significantly enhanced photocatalytic performance of ZnO via graphene hybridization and the mechanism study," *Applied Catalysis B*, vol. 101, no. 3-4, pp. 382–387, 2011.

[36] H. Kim, J. T. Baek, and H. H. Park, "A study of the electrical properties of graphene-incorporated direct-patternable ZnO thin films," *Thin Solid Films*, vol. 529, pp. 234–2237, 2013.

[37] A. Prakash, S. K. Misra, and D. Bahadur, "The role of reduced graphene oxide capping on defect induced ferromagnetism of ZnO nanorods," *Nanotechnology*, vol. 24, Article ID 095705, 2013.

[38] J. Wang, B. Li, J. Chen et al., "Diethylenetriamine-assisted synthesis of CdS nanorods under reflux condition and their photocatalytic performance," *Journal of Alloys and Compounds*, vol. 535, pp. 15–20, 2012.

[39] H. N. Lim, R. Nurzulaikha, I. Harrison et al., "Preparation and characterization of tin oxide, SnO_2 nanoparticles decorated graphene," *Ceramics International*, vol. 38, no. 5, pp. 4209–4216, 2012.

[40] N. Xu, Z. Shi, Y. Fan, J. Dong, J. Shi, and M. Z.-C. Hu, "Effects of particle size of TiO_2 on photocatalytic degradation of methylene blue in aqueous suspensions," *Industrial and Engineering Chemistry Research*, vol. 38, no. 2, pp. 373–379, 1999.

[41] F. Ye, Y. Peng, C. Guang-Yi, B. Deng, and X. An-Wu, "Facile solution synthesis and characterization of ZnO mesocrystals and ultralong nanowires from layered basic zinc salt precursor," *Journal of Physical Chemistry C*, vol. 113, no. 24, pp. 10407–10415, 2009.

[42] R. Kou, Y. Shao, D. Wang et al., "Enhanced activity and stability of Pt catalysts on functionalized graphene sheets for electrocatalytic oxygen reduction," *Electrochemistry Communications*, vol. 11, no. 5, pp. 954–957, 2009.

[43] A. A. Más and D. Wei, "Photoelectrochemical properties of graphene and its derivatives," *Nanomaterials*, vol. 3, pp. 325–356, 2013.

[44] J. Durantini, P. P. Boix, M. Gervaldo et al., "Photocurrent enhancement in dye-sensitized photovoltaic devices with titania-graphene composite electrodes," *Journal of Electroanalytical Chemistry*, vol. 683, pp. 43–46, 2012.

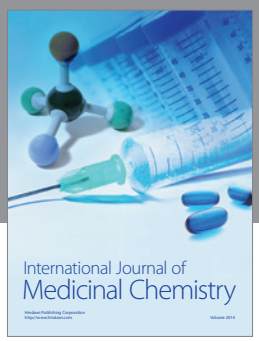

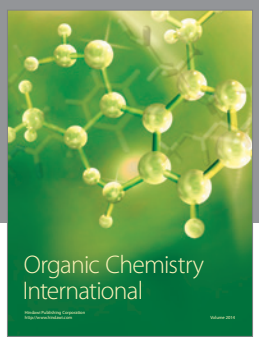

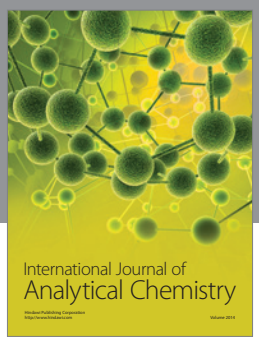

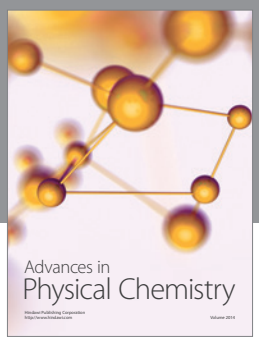

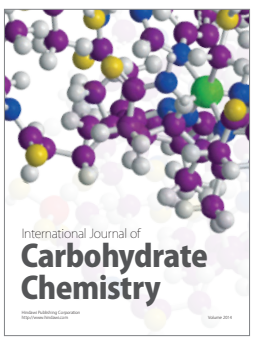

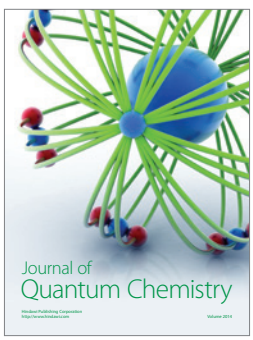

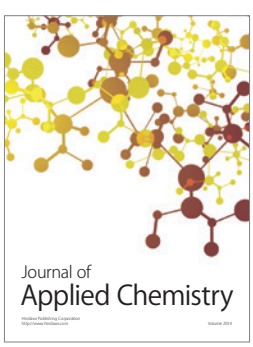

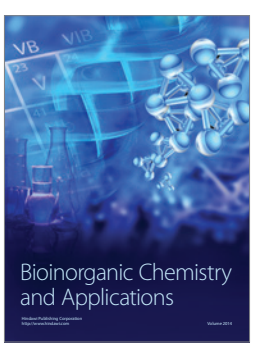

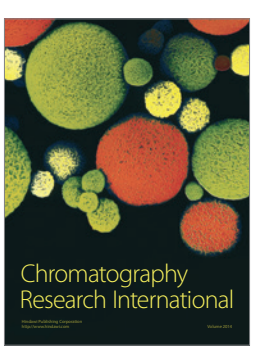

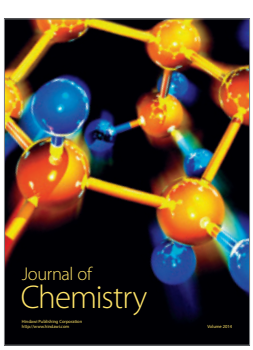

Hindawi

Submit your manuscripts at
http://www.hindawi.com